Int. J. Electrochem. Sci., 14 **(2019)** 5462 – 5471, doi: 10.20964/2019.06.69

International Journal of
ELECTROCHEMICAL
SCIENCE
www.electrochemsci.org

The Electrochemical Performance of Ferrosilicon Master Alloy as Anode Material for Lithium-Ion Batteries

Lin Wu, Xinlin Zhang, Liwu Huang[*]*, Yungui Chen*[*]

College of Materials Science and Engineering, Sichuan University, Chengdu 610065, PR China
[*]E-mail: liwuhuang@scu.edu.cn, ygchen60@aliyun.com

Received: 16 February 2019 / *Accepted:* 9 April 2019 / *Published:* 10 May 2019

Alloy electrode has greatly improved the low Li^+/electron conductivity and relieved the huge volume expansion of Si via using elastic inactive matrix to accommodate the active component. Here we choose ferrosilicon master alloy (FS) used widely in the metallurgical industry as possible negative electrode materials with Si as active center and highly conductive FeSi phase as elastic matrix. The carbon coating ferrosilicon (FSC) anode exhibits a good cycle performance of 430 mAh g^{-1} after 100 cycles and a good rate performance of 400 mAh g^{-1} at a current density of 1000 mA g^{-1}. To confirm the charge/discharge reaction mechanism, XRD was applied to detect the phase changes of the anode during the first three reaction processes. It can be seen from the results that the amorphous carbon layer and FeSi phase can act as a buffer layer to relax the stress of Si and improve the electrical conductivity among Si particles during cycling.

Keywords: ferrosilicon; lithium-ion batteries; reaction mechanism; anode

1. INTRODUCTION

Lithium-ion batteries are now the most common used power sources for electric vehicles and portable electronic devices. To meet the increasing demand of batteries with higher specific energy, the development of advanced anode materials is just around the corner.

Due to its high theoretical capacity ($Li_{4.4}Si$, up to 4200 mAh g^{-1}), good safety, environmental friendliness and low operating voltage (0.4 V), silicon is considered to be an attractive anode material.[1-3]. However, one of the obstacles for its commercialization is the severe volume change during the charge/discharge process, resulting in the poor cyclability. Another is its low electrical conductivity[4-6].

To alleviate these problems, many efforts have been made such as making nano-size particles[7], preparing Si-based composite with stable matrix[8], and designing porous structure, hollow structure, core-shell structure, yolk-shell structure Si materials[9-12]. Also, carbon coating is an effective method

to improve electrical conductivity and provide ample Li^+ transport channels[13].

It is confirmed that making nano-size particles cannot improve the cyclability of the Si materials effectively[14], because the nano-size particles may aggregate to reunite after a few cycles. However, using elastic inactive matrix to accept the active component is likely to be an effective way to relieve the volume expansion of the alloy electrodes[15]. Ferrosilicon is widely used in steel industry, foundry industry and other industrial production on account of its mature manufacturing process and low cost. For the past few years, some Fe-Si anodes are reported for Lithium-ion batteries. But most of the Fe-Si anodes are synthesized by ball-milling Si and Fe power[16, 17], which are high cost and time-consuming.

In our work, we choose FeSi 75 (~ 73.3 wt % Si, ~ 21.4 wt % Fe, FS) master alloy as possible negative electrode materials with Si as active center and FeSi phase as elastic matrix, where the FSC composite is obtained by using dopamine as a carbon source coated on its surface. This paper covers the preparation and the electrochemical performance of FSC composite anode compared with commercial Si and the discussion about the charge/discharge mechanism of FSC material.

2. EXPERIMENTAL

2.1 Materials preparation

The synthetic process of the FSC nanocomposite is depicted in Fig. 1. The ferrosilicon (73.3 % Si, 21.4 % Fe and other impurities, such as Mn, Al, Henan Star Metallurgy Material Co. Ltd., China) as the silicon source was used to prepare the active anode materials. Commercial silicon nanoparticles (100 nm in diameter) were bought from Shanghai Chaowei Nano Technology Co. Ltd., China. Firstly, the bulk FS alloy was crushed into powder followed by adding 3 ml of anhydrous ethanol and then milled by ball-milling. The weight ratio of balls to materials was 20:1. We prepared FS powder under different milling time including 1 h, 3 h, 6 h, and marked them as FS-1, FS-3 and FS-6. The milled alloy powders were firstly dispersed in the mixture solution of Tris-buffer (200 mL, 10 mM, pH=8.5) and ethanol (20 mL) for 30 min. And then, continue to add 0.36 g dopamine into the above mixture. The reactions were implemented under continual magnetic stirring for 18 h. Next, the obtained product was washed several times by deionized water and ethanol to get a neutral solution, and then dried at 60 °C for 12 h. Finally, the dried product was calcined in the tube furnace under N_2 condition at 600 °C for 2 h with a heating rate of 5 °C min^{-1} to obtain the carbon coating ferrosilicon (FSC), FSC-3 represents the carbon coating FS-3 in this paper.

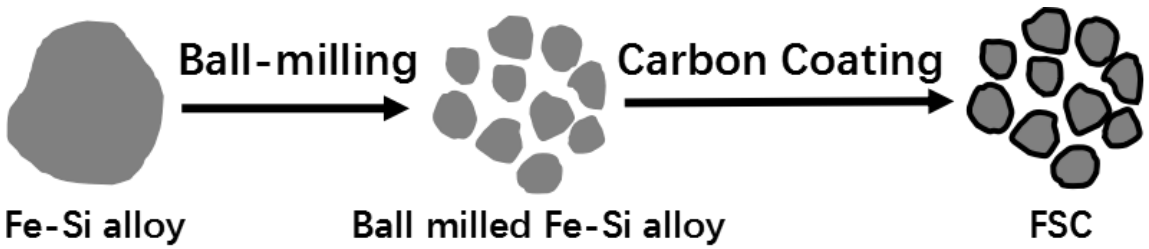

Figure 1. Schematic illustration of synthesizing FSC anode materials

2.2 Materials characterizations

For the purpose of detecting the phase composition of the composites, X-ray diffraction (XRD, DX-2600, Cu Kα radiation, λ = 1.54178 Å) analysis was used at a step scanning of 4 °min^{-1} from 10° to 80° in the 2θ range. X-ray photoelectron spectroscopy (XPS) analysis was carried out using PHI Quantera XPS. The content of carbon in the composite was measured under air atmosphere by thermal gravimetric analysis (METTLER TOLEDO TGA/DSC2) with a ramping speed of 10 °C min^{-1} from room temperature to 800 °C. The crystal surface morphology was detected via the scanning electron microscope (SEM, JEOL JSM-7800F).

2.3 Electrochemical measurements

Coin cells (type 2025) were assembled to test the electrochemical performance. The FSC powers were mixed with 20 wt % acetylene black (AB) as a conductive additive and 10 wt % Sodium alginate (SA) as a binder. The obtained slurry was spread on a Cu-foil using a blade coater, and then dried at 80 °C under vacuum overnight. The areal density of the anodes for each electrode was about 1.5~1.6 mg cm^{-2}. The electrolyte was 1 M $LiPF_6$ in a mixture of ethylene carbonate (EC) and dimethyl carbonate (DMC) (1:1 in volume) with fluoroethelene carbonate(FEC) additive(5 wt %). The half-cell was assembled in an Ar-filled glove-box with a lithium metal foil as the counter electrode. The disassembly of the cell was also performed in an Ar-filled glove-box, using 1,2-dimethoxyethane(DME) as a solvent to scrap off the powder. All the electrochemical experiments were tested with a multichannel battery-testing system (LAND CT 2001 A, Wuhan LAND electronics Co., China) and carried out in a galvanostatic mode with a potential range of 0.01-1.5 V vs Li^+/Li. All the electrochemical tests were performed at about 25 °C. The capacity was calculated on the basis of the total mass of the composite active materials. Cyclic voltammetry (CV) was tested using electrochemical workstation (PARATAT 2273) with a scan rate of 0.1 mV s^{-1} between 0.01-1.5 V for 3 cycles. Electrochemical impedance spectroscopic (EIS) test was obtained using electrochemical workstation with the frequency range of 1 MHz to 0.01 Hz and the amplitude of 5 mV.

3. RESULTS AND DISCUSSION

The phase composition characterization of the samples by XRD is shown in Fig. 2(a). It clearly demonstrates the presence of $FeSi_2$(JCPDS No. 35-0822), FeSi (JCPDS No. 89-7376)[18] and Si (JCPDS No. 27-1402)[19]. It is evident that all the samples show very similar diffraction peaks. The sharp peaks of the sample are observed at 28.3, 47.4, 56.2, 69.3 and 76.4°, which accord perfectly with the (111), (220), (311), (400) and (331) lattice planes of crystallized silicon, respectively[20]. As the ball milling time increases, the peaks become broad, which is probably due to sample refinement and lattice internal strain.

To further clarify the content of the carbon in FSC-3, thermogravimetric (TG) analysis was conducted in the air. As shown in Fig. 2(b), the distinct weight loss from 350 °C to 600 °C is due to the

oxidation and combustion of carbon under air atmosphere, while the tiny weight loss before 350 °C could be mainly due to the evaporation of adsorbed water[21]. Si particles in the FSC composite exhibits a thermal stability below 800 °C. According to the TG curve, the carbon content of FSC-3 can be calculated to be about 9%.

XPS measurement was taken to examine the chemical composition of the surface on FSC composite. The survey scan spectrum of the FSC-3 composites confirms the presence of C and N (Fig. 2(c)). Due to the fact that dopamine is a nitrogenous carbon source, three peaks located at 401.2, 399.7 and 398.3 eV are well fitted to the N 1 s spectrum in Fig. 2(d), indicating the existence of the graphitic, pyrrolic and pyridinic nitrogen doped into the carbon structure, respectively. Nitrogen-doped carbon can not only optimize the electrical conductivity by providing ample free electrons, but also enhance the mechanical stability of the carbon structure during charge/discharge process[22]. Since the detection depth of XPS is only a few nanometers and the carbon coating may be intact in the surface, no Si and Fe were detected.

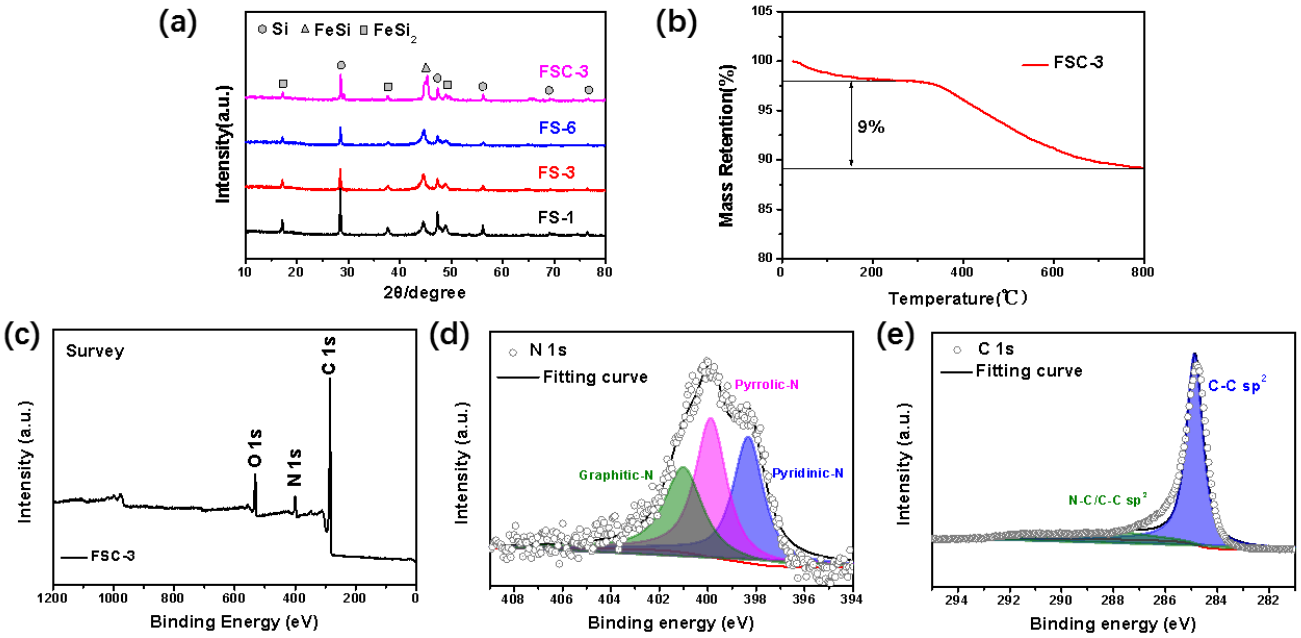

Figure 2. (a) XRD patterns of FS-1, FS-3, FS-6 and FSC-3, (b) TG curve of the FSC-3, XPS spectra of the FSC-3: (c) survey, (d) N 1s, (e) C 1s.

The microstructure and morphological features of the FSC material can be seen from its scanning electron microscopy (SEM) images given in Fig. 3(a), (b) and (c) from those after 1 h, 3 h and 6 h of milling, respectively. With the increase of milling time, the size of particles becomes small, but the FS-6 particles (Fig. 3(c)) have slight agglomeration. And the particle size is in the range of dozens of nanometers to one micrometer, which ensures the integral uniformity of the material. After 3 h, the particle size does not decrease significantly with the ball-milling time prolonged. In order to save cost and improve the electrochemical performance, we choose FS-3 to coat carbon. After carbon coating process, the particles show more uniform particle size distribution and better dispersion (as shown in Fig. 3(d)).

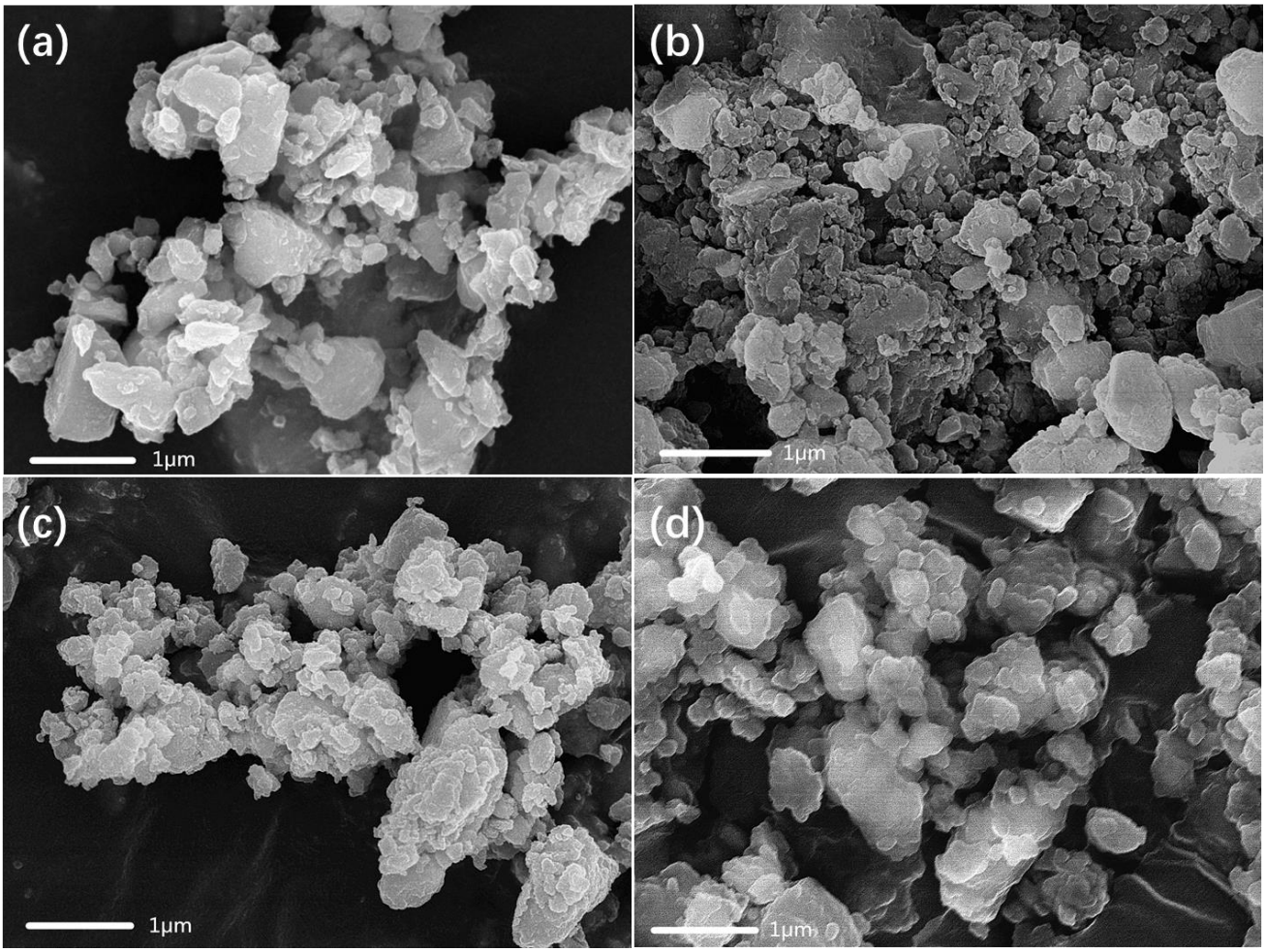

Figure 3. SEM images of (a) FS-1, (b) FS-3, (c)FS-6 and (d) FSC-3.

Fig. 4(a) shows the discharge−charge voltage curves of FSC-3 composite electrode at a current density of 200 mA g^{-1}. In the first cycle, the plateau at around 0.7 V is related to the formation of the solid electrolyte interphase (SEI) film. The FSC electrode shows a very flat plateau at around 0.1 V, which is correspond to the lithiation of crystal Si (c-Si) [21]. And the first charge plateau at about 0.45 V corresponds to the characteristic plateau of the amporphous Si (a-Si) from Li_xSi phase. The FSC composite shows the first discharge/charge capacities of 1092/680 mAh g^{-1}, with an initial coulombic efficiency of 62 %. It is well-known that there always exists a large irreversible capacity attributed to the electrochemical reduction of electrolyte with Li^+ for the irreversible SEI film formation and the partial inactivation of inserted lithium in the Si anodes during the lithium ion intercalation process[16]. After the initial cycle, c-Si is electrochemically transformed into amorphous one. As a result, the FSC composite shows a plateau at about 0.2 V in the subsequent cycles, corresponding to the typical lithiation plateau of a-Si to Li_xSi. For a Si-based anode, both c-Si and a-Si are lithium reaction active[18]. However, a-Si has better pulverization resistance because of the smaller volume expansion upon Li insertion [23]. The structure becomes more stable since the second cycle, the coulombic efficiency of the electrode increases rapidly to 93 % and arrived at ≥ 99 % after 5 cycles. The 2nd and 3rd cycles are almost overlapping, which indicates that the FSC anodes have superior stability and cyclability.

To further confirm the charge/discharge mechanism, XRD was applied to test the phase changes of the composite electrode during the first three cycles. Five points were taken from the first three charge/discharge curves (Fig. 4(a)), 0.7 V, 0.1 V, 0.01 V, 0.45 V and 1.5 V, respectively. It could be seen from Fig. 4(b), the initial electrode includes Si phase, FeSi phase and $FeSi_2$ phase, with the insertion of Li^+, the XRD peaks of Si phase and $FeSi_2$ phase decreased at the same time and disappeared at 0.01 V. In subsequent cycling, no XRD peaks of Si phase and $FeSi_2$ phase could be measured. The same phenomenon is discovered in the research of lithium insertion into silicon[24], which is due to the irreversible transform of Si phase from crystalline to amorphous state. This mechanism may also apply to FS alloy. Apart from these XRD features, it is worth noting that the FeSi phase remains constant during charge/discharge cycle, suggesting that FeSi phase serves as an inert and electrically conductive matrix to relax the stress of Si and to improve the electronic conduction among Si particles. On account of these results, the reaction process formula of the FSC composite can be depicted as:

First lithiation $\quad c\text{-}Si+FeSi_2+FeSi+xLi^+ \rightarrow Li_{15}Si_4+FeSi$ $\quad$ Equation (1)

First delithiation $\quad Li_{15}Si_4+FeSi \rightarrow a\text{-}Si+Li+FeSi$ $\quad$ Equation (2)

Subsequent cycle $\quad a\text{-}Si+xLi^++FeSi \leftrightarrow a\text{-}Li_xSi+FeSi$ $\quad$ Equation (3)

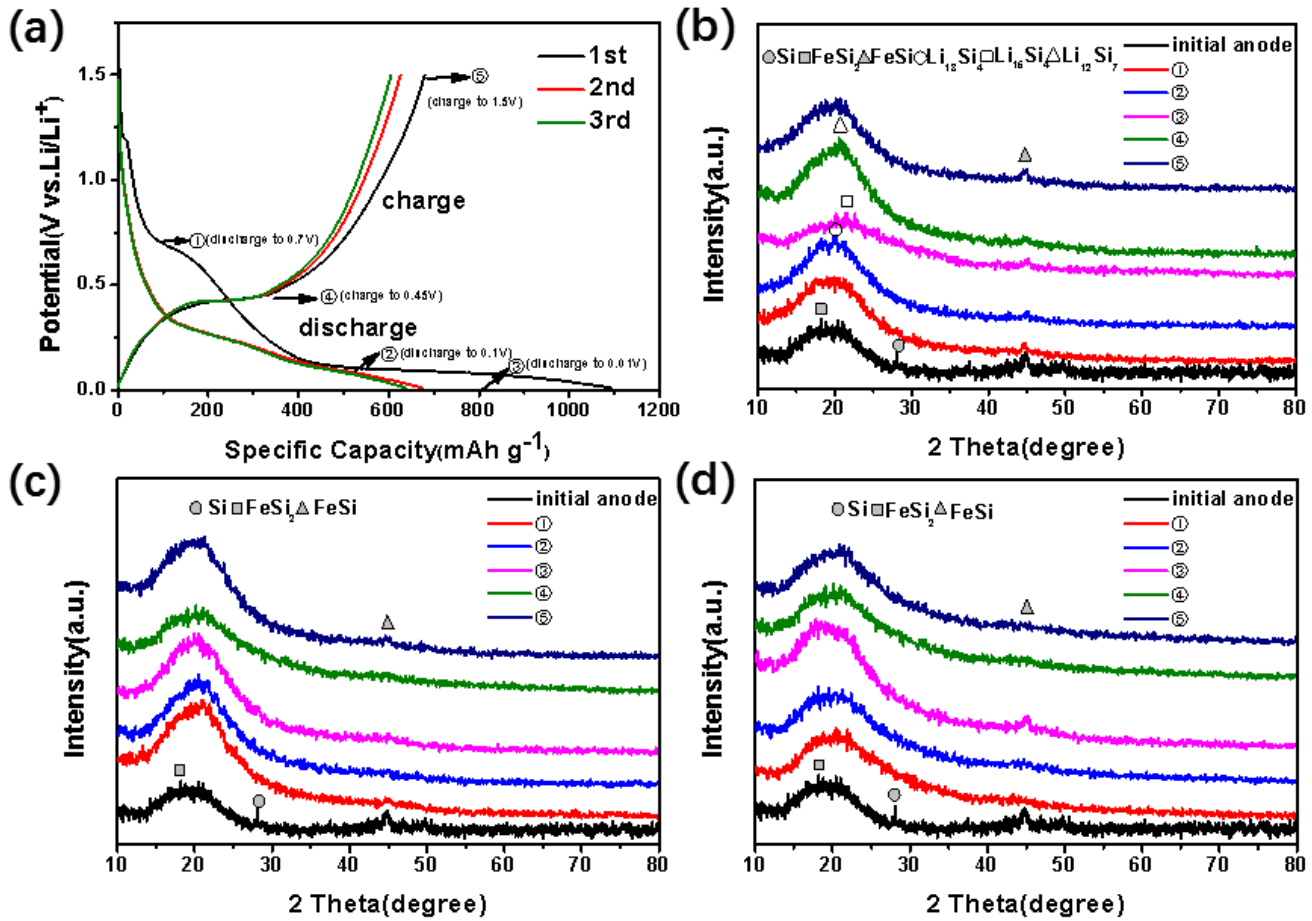

Figure 4. (a) Charge-discharge curves of FSC-3, XRD patterns of (b) the first cycle, (c) the second cycle, (d) the third cycle

We measured cyclic voltammetry (CV) of the Si, FS and FSC materials to study the

electrochemical Li-alloying reactions at a scanning rate of 0.1 mV s^{-1} from 1.5 to 0.01 V versus Li^+/Li as shown in Fig. 5(a), (b), (c). It can be seen from Fig. 5(a) that the intensities of the Si anodic peaks are gradually reduced with the cycle number increasing, indicating that the Li-ion reaction between Li^+ and active silicon is sluggish, which can be due to the transformation of the active Si from crystal to amorphous as well as the formation of the thick SEI. However, in FS-3 (Fig. 5(b)), the intensities of the Si anodic peaks are observed to be almost similar after the first cycle, because of the well contact between Si and stable SEI formation. As for FSC-3 in Fig. 5(c), in the first cathodic scan starting from 1.5 to 0.01 V, when the potential scan goes lower to 0.1 V, an obvious and sharp reduction peak is observed at a low potential of about 0.01 V, which is attributed to the lithiation of crystalline Si to form the Li_xSi phase. This peak corresponds to the Equation (1). In the following anodic scan, two oxidation peaks appeared at 0.34 and 0.52 V, which corresponded to a two-steep dealloying process of Li_xSi phase. Since the second cycle and thereafter, a new peak appears at 0.19 V on the cathodic scan, which corresponds to the lithiation of amorphous Si. The location of the anodic and cathodic peaks basically remains unchanged, confirming that a stable SEI layer has been formed and that there could be no other reactions in the subsequent cycles, indicating an excellent cyclability. With the increasing of cycle number, the intensity of the peaks increase, which is due to the electrolyte infiltration and the activation of materials in accordance with the discharge−charge voltage curves.

Electrochemical impedance spectroscopy (EIS) were also conducted for all samples. As shown in Fig. 5(d), the proposed equivalent circuit is presented as inset[25]. All the materials exhibit similar Nyquist plots, in which the semicircle diameter associated with the charge transfer resistance (Rct) at the SEI layer in the high frequency region, while the low frequency sloping slash corresponds to the ion diffusion resistance in the active material, called Z_w. Z_w usually shows the difficulty of the Li-ion diffusing into the particle. As shown in Fig. 5(d), the gradient of Si is lower than that of FS and FSC sample, indicating that the Li-ion diffusing into the FS and FSC is easier. The FSC shows a smaller semicircle than those of the FS and Si, which indicates a lower R_{ct} in the FSC than in the FS and Si, because the diameter of semicircle grows with R_{ct}. This result indicates that the FSC anode has a more stable SEI film than FS and Si, as well as better charge transfer kinetics on the surface, because the nitrogen-doped carbon shell includes numerous micropores, which provides plenty of charge-transfer channels at the interface of electrode and electrolyte.

Fig. 5(e) evaluates the cycling performance of the FSC composite electrodes for different periods after the first two activation cycles at 100 mA g^{-1}, the current density gradually increased to 200 mA g^{-1} for the following cycles with those using FS alone and commercial Si alone for comparison. We consider that there is no significant influence in the discharge capacities of FS-3 and FSC-3 electrodes because the capacity of FeSi is within 20 mAh g^{-1} [26]. As expected, the commercial Si exhibits promising electrode performance with the highest initial capacity of 2721 mAh g^{-1} while the capacity of FS and FSC are 1157 and 1018 mAh g^{-1}. But the discharge capacity of commercial Si electrode decreases quickly in the first 20 cycles. For the initial 20 cycles, the FS material shows smaller capacities than the commercial Si. This is due to the existence of electrochemically inactive FeSi phase in the FS. However, the capacity reducing is much lower for the FS than for the Si one, indicating the improvement of cyclability. Although the first reversible capacity of FS anode is high, after 30 cycles, its capacity quickly decreases to < 400 mAh g^{-1}, indicating a very low capacity retention of only 36.7 %, whereas the

reversible capacity of FSC composite electrode is of about 600 mAh g^{-1} after 30 cycles, corresponding to an excellent capacity retention of 60 % with respect to those of the commercial Si and FS. Meanwhile, the coulombic efficiency keeps stable at 99 % after 10 cycles. After 20-25 cycles, the capacity of the FSC composite electrodes exceeds that of the commercial Si and FS electrode. The excellent cyclability of the FSC composite is possibly due to two reasons: (1) the inert conductive FeSi phase in the Si can effectively relieve the volume expansion of pristine Si during lithiation while also improve the electrical conductivity of the pristine Si[27] (2) The carbon layer serves as a buffer layer to further alleviate the mechanical stress and also forms stable SEI film on the surface to reduce consuming Li^+ during charge and discharge cycles.

The rate characteristics of the Si, FS-3 and FSC-3 composite electrodes are given in Fig. 5(f). When the current densities increased successively from 50 mA g^{-1} to 100 mA g^{-1} and further to 5 A g^{-1}, the capacities of the FSC-3 reduce slightly from 1178 mAh g^{-1} to 621 mAh g^{-1} and 233 mAh g^{-1}. The FSC shows better high-rate capability than the FS and Si. The FSC material can still retain a promising reversible capacity of about 400 mAh g^{-1} even at a high current density of 1 A g^{-1}. When the current density was reduced back to 100 mA g^{-1}, the capacity of 600 mAh g^{-1} can be retained. Apparently, the large rate capability of the FSC composite benefits from the stability, excellent electrical conductivity of FeSi phase and the coating of carbon layer that provides not only greatly optimizing electrical conductivity but also ample Li^+ transport channels.

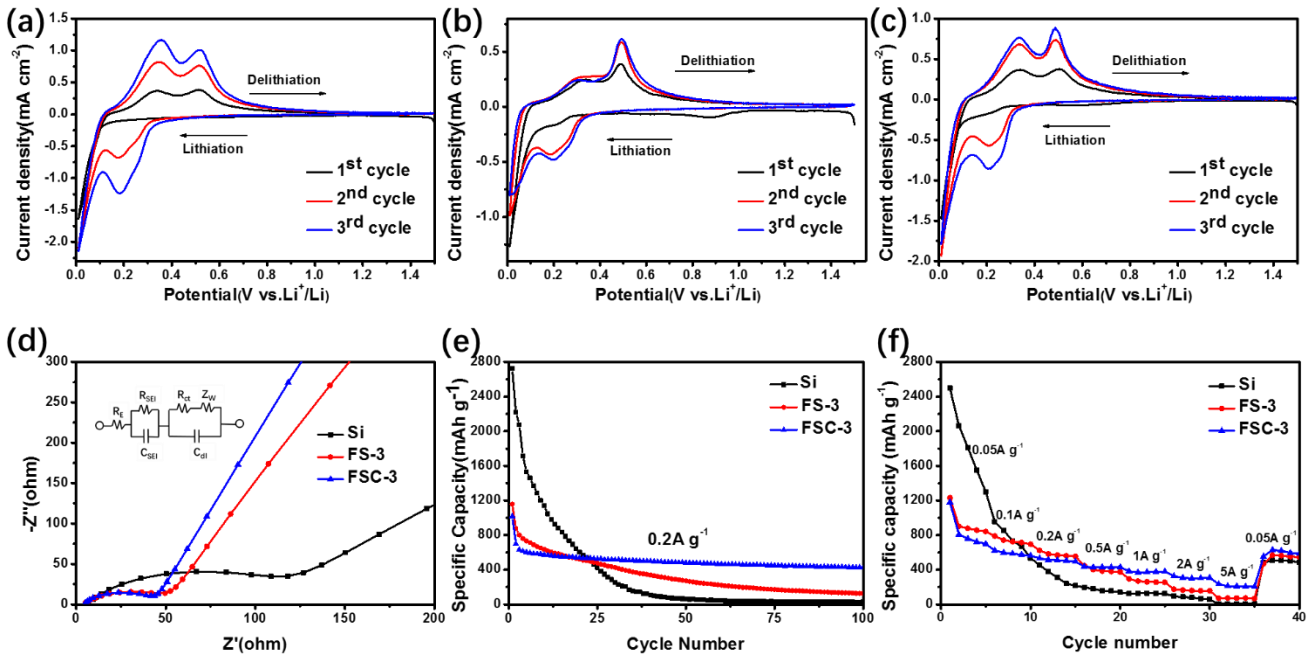

Figure 5. CV profiles of (a) Si (b) FS-3 and (c) FSC-3, (d) electrochemical impedance spectra of Si, FS-3 and FSC-3, (e) cycling performance of Si, FS-3 and FSC-3, (f) rate performance of Si, FS-3 and FSC-3

Table 1. Summary of the electrochemical performance of previous lithium-ion batteries based on ferrosilicon anodes compared to this work

Ferrosilicon based anodes	Source	Carbon coating method	Highest capacitances obtained	Refs
Graphite–$Fe_{20}Si_{80}$	Commercial Si and Fe powder	Planetary mill for 0.5–2 h	800 mAh g^{-1}	[17]
$FeSi_2$/Si@C	Commercial Si and Fe powder	Planetary mill for 6 h	1296 mAh g^{-1}@ 100 mA g^{-1}	[16]
Fe–Si/C	Ferrosilicon	Planetary mill for 10 h	680 mAh g^{-1}@ 100 mA g^{-1}	[15]
FSC	Ferrosilicon	Planetary mill for 12 h	1500 mAh g^{-1}@ 50 mA g^{-1}	[13]
Fe–Si@C	Ferrosilicon	Chemical	1018 mAh g^{-1}@ 100 mA g^{-1}	This work

As can be seen from Table 1, there are two sources of ferrosilicon based anodes, one is prepared by ball milling of commercial silicon and iron power, and the other is directly using industrial ferrosilicon alloy. It can be seen that ferrosilicon is more economical and convenient, and the electrochemical performance of the prepared anode is similar to that of the ball milling one. From the way of composition with carbon, the method of planetary ball milling is adopted, while this method consumes a large amount of energy and the loss of raw materials is also serious. Therefore, we use ferrosilicon as the raw material and chemical method for carbon coating, which makes the preparation process simple and suitable for industrial production.

4. CONCLUSIONS

In conclusion, we have successfully synthesized the FSC composite directly from industrial ferrosilicon master alloy, using an economical and convenient method by straightforward ball-milling and chemical method for carbon coating process. The as-prepared FSC anode shows a good cycle performance of 430 mAh g^{-1} after 100 cycles and a good rate property of 400 mAh g^{-1} at a current density of 1 A g^{-1}. It can be seen from the charge/discharge reaction mechanism, the FeSi phase remains constant during charge/discharge cycle, suggesting that FeSi phase serves as an inert and electrically conductive buffering matrix to relax the stress of Si and to improve the electronic conduction between Si particles. Most importantly, the synthetic route of this anode materials is simple and cost-effective, enabling it is commercially viable for large-scale production. The reaction mechanism of ferrosilicon has important significance, and is worthy of further study.

References

1. X. Su, Q. Wu, J. Li, X. Xiao, A. Lott, W. Lu, B.W. Sheldon, J. Wu, *Adv. Energy Mater,* 4 (2014) 1300882.
2. X. Li, M. Gu, S. Hu, R. Kennard, P. Yan, X. Chen, C. Wang, M.J. Sailor, J.G. Zhang, J. Liu, *Nat Commun,* 5 (2014) 4105.
3. K. Adpakpang, J.-e. Park, S.M. Oh, S.-J. Kim, HwangSeong-Ju, *Electrochimica Acta*, 136 (2014) 483.
4. U. Kasavajjula, C. Wang, A.J. Appleby, *Journal of Power Sources,* 163 (2007) 1003.
5. E. Hüger, L. Dörrer, H. Schmidt, *Chem. Mater,* 30 (2018) 3254.
6. X. Liu, L. Zhong, S. Huang, S.X. Mao, T. Zhu, J. Huang, *acsnano,* 6 (2012) 1522.
7. K. Liang, H. Yang, W. Guo, J. Du, L. Tian, X. Wen, *Journal of Alloys and Compounds,* 735 (2018) 441.
8. Y.M. Yang, C. Loka, D.P. Kim, S.Y. Joo, S.W. Moon, J.H. Park, *Met. Mater. Int,* 23 (2017) 610.
9. N. Liu, H. Wu, M.T. McDowell, Y. Yao, C. Wang, Y. Cui, *Nano Letters,* 12 (2012) 3315.
10. Y. Yao, M.T. McDowell, I. Ryu, H. Wu, N. Liu, L. Hu, W.D. Nix, Y. Cui, *Nano Letters,* 11 (2011) 2949.
11. R. Zhou, R. Fan, Z. Tian, Y. Zhou, H. Guo, L. Kou, D. Zhang, *Journal of Alloys and Compounds,* 658 (2016) 91.
12. H. Tian, X. Tan, F. Xin, C. Wang, W. Han, *Nano Energy,* 11 (2015) 490.
13. W. He, Huajun Tian , Shunlong Zhang, H. Ying, Z. Meng, W. Han, *Journal of Power Sources,* 353 (2017) 270.
14. H. Li, X.J. Huang, L.Q. Chen, G.W. Zhou, Z. Zhang, D.P. Yu, Y.J. Mo, N. Pei, *Solid State Ionics,* 135 (2000) 181.
15. H. Dong, R.X. Feng, X.P. Ai, Y.L. Cao, H.X. Yang, *Electrochimica Acta,* 49 (2004) 5217.
16. Y. Chen, J. Qian, Y. Cao, H. Yang, X. Ai, *Appl. Mater. Interfaces,* 4 (2012) 3753.
17. H.Y. Lee, S.M. Lee, *Journal of Power Sources,* 112 (2002) 649.
18. M. Gao, D. Wang, X. Zhang, H. Pan, Y. Liu, C. Liang, C. Shang, Z. Guo, *J. Mater. Chem. A,* 3 (2015) 10767.
19. J. Xie, L. Tong, L. Su, Y. Xu, L. Wang, Y. Wang, *Journal of Power Sources,* 342 (2017) 529.
20. X. Zhuang, Y. Zhang, L. He, Y. Zhu, Q. Shi, Q. Wang, G. Song, X. Yan, *Journal of Alloys and Compounds,* 731 (2018) 1.
21. Y. Ma, H. Tang, Y. Zhang, Z. Li, X. Zhang, Z. Tang, *Journal of Alloys and Compounds,* 704 (2017) 599.
22. X. Zhou, K. Han, H. Jiang, Z. Liu, Z. Zhang, H. Ye, Y. Liu, *Electrochimica Acta,* 245 (2017) 14.
23. B. Jerliu, L. Dorrer, E. Huger, G. Borchardt, R. Steitz, U. Geckle, V. Oberst, M. Bruns, O. Schneider, H. Schmidt, *Phys Chem Chem Phys,* 15 (2013) 7777.
24. M.N. Obrovaca, L.J. Krause, *Journal of The Electrochemical Society,* 154 (2007) A103.
25. X. Zhang, L. Huang, P. Zeng, L. Wu, Q. Shen, *Chemical Engineering Journal,* 357 (2019) 625.
26. H. Usui, K. Meabara, K. Nakai, H. Sakaguchi, *Int. J. Electrochem. Sci.,* 6 (2011) 2246.
27. I.J. Jo, J.A. Ha, W.W. Park, K.Y. Sohn, *Journal of the Korean Physical Society,* 67 (2015) 1937.